part of the potential in the 200-400 MeV bombarding energy range). We refer specifically to the treatment of the nucleon-nucleon interaction in nuclear matter in terms of a Brueckner-Hartree-Fock (BHF) expansion, and its application to finite nuclei via a local density approximation,[1-3] and to an independent relativistic approach starting from the Dirac-Hartree (DH) model using scalar and vector meson exchange NN interactions.[4,5] These models predict that the real central potential exhibits roughly a WS shape at low energies (E < 100 MeV), but gradually develops a characteristic central depression (the "wine-bottle-bottom" shape) as the bombarding energy is raised toward 200 MeV.

A systematic analysis of the ^{9}Be, ^{12}C, ^{16}O and ^{28}Si data is underway to determine the extent to which phenomenological WS and non-WS (e.g., double-WS) potential forms can describe the data. The results of this analysis are expected soon. The data will also be compared with predictions of the BHF and DH microscopic optical models.

1) C. Mahaux, Proc. Conf. on Microscopic Optical Potentials, Hamburg, 1978, p. 1.

2) F.A. Brieva and J.R. Rook, Nucl. Phys. A291, 299 and 317 (1977).

3) H.V. von Geramb, F.A. Brieva, and F.R. Rook, Proc. Conf. on Microscopic Optical Potentials, Hamburg, 1978, p. 104.

4) L.G. Arnold, B.C. Clark, R.L. Mercer, and P. Schwandt, to be published in Phys. Rev. C (in press).

5) P. Schwandt, L.G. Arnold, B.C. Clark, R.L. Mercer, IUCF Scientific and Technical Report 1980, p. 7.

6) H.O. Meyer, P. Schwandt, G.L. Moake, and P.P. Singh, Phys. Rev. C 23, 616 (1981).

7) A.D. Bacher, G.T. Emery, W.P. Jones, D.W. Miller, C. Olmer, P. Schwandt, S. Yen, R.J. Sobie, T.E. Drake, W.G. Love, and F. Petrovich, IUCF Scientific and Technical Report 1980, p. 26.

8) P. Schwandt, H.O. Meyer, W.W. Jacobs, A.D. Bacher, S.E. Vigdor, M.D. Kaitchuck, to be published in Phys. Rev. C.

ANALYZING POWER OF PROTON-NUCLEUS ELASTIC SCATTERING BETWEEN 80 AND 180 MEV AND THE OPTICAL POTENTIAL

P. Schwandt, H.O. Meyer, W.W. Jacobs, A.D. Bacher, S.E. Vigdor, and M.D. Kaitchuck
Indiana University Cyclotron Facility, Bloomington, Indiana 47405

T.R. Donoghue
Ohio State University, Columbus, Ohio 43212

For proton-nucleus scattering, the importance of the projectile spin-dependent interaction increases dramatically relative to the central interaction as one increases the bombarding energy to the medium-energy range. For example, a previous investigation focusing on cross-section $\sigma(\theta)$ measurements[1] showed a surprising sensitivity of $\sigma(\theta)$ to the spin-orbit potential, manifested in a pronounced damping of the characteristic diffractive oscillations at intermediate angles for bombarding energies greater than ~100 MeV. Although the spin-orbit potential parameters were better defined by the cross-section measurements than expected, appreciable ambiguities and uncertainties remained. Both additional and higher-quality polarization data were called for in order to refine the parametrization of the spin-dependent potential in this energy regime.

This report presents the final results of an experimental program in proton-nucleus elastic scattering between 80 and 180 MeV carried out with a polarized proton beam at the Indiana University Cyclotron Facility. The 16 data sets presented here are restricted to measurements of the analyzing power $A_y(\theta)$ since most of the corresponding cross section angular distributions have already been reported in the literature.[1] The $\sigma(\theta)$ and $A_y(\theta)$ data have been

analyzed within the framework of a conventional optical potential model and the behavior of the potential parameters as a function of energy is investigated.

Details of the experimental procedure and a discussion of the systematic energy and target mass dependences of the analyzing power (as well as of the associated, previously reported differential cross section) in terms of an interplay between the partial cross sections for scattering of protons with spin up or down with respect to the scattering plane can be found in a paper[2] on this work submitted for publication in Physical Review C. The data presented here include analyzing-power measurements $A_y(\theta)$ made at IUCF for 80-180 MeV protons elastically scattered from a number of targets, ranging from ^{24}Mg to ^{208}Pb. In some cases, for completeness, a comparison is made with angular distributions of $A_y(\theta)$ obtained at other institutions.[3-5] These data are illustrated in Figs. 1-3. Although the present experiment yielded cross section data as well as analyzing powers, the cross-section angular distributions used in the present optical model analysis were taken from a more complete earlier experiment at IUCF using an unpolarized beam.[1] In two cases, $\sigma(\theta)$ data obtained at Maryland[6] were adopted. The results for elastic scattering from the nuclei ^{24}Mg, ^{28}Si, ^{92}Zr and ^{120}Sn have been obtained as the byproduct of inelastic proton scattering measurements, not specifically aimed at observing the ground state transition. These experiments were mainly concerned with exploring the giant resonance region[7]

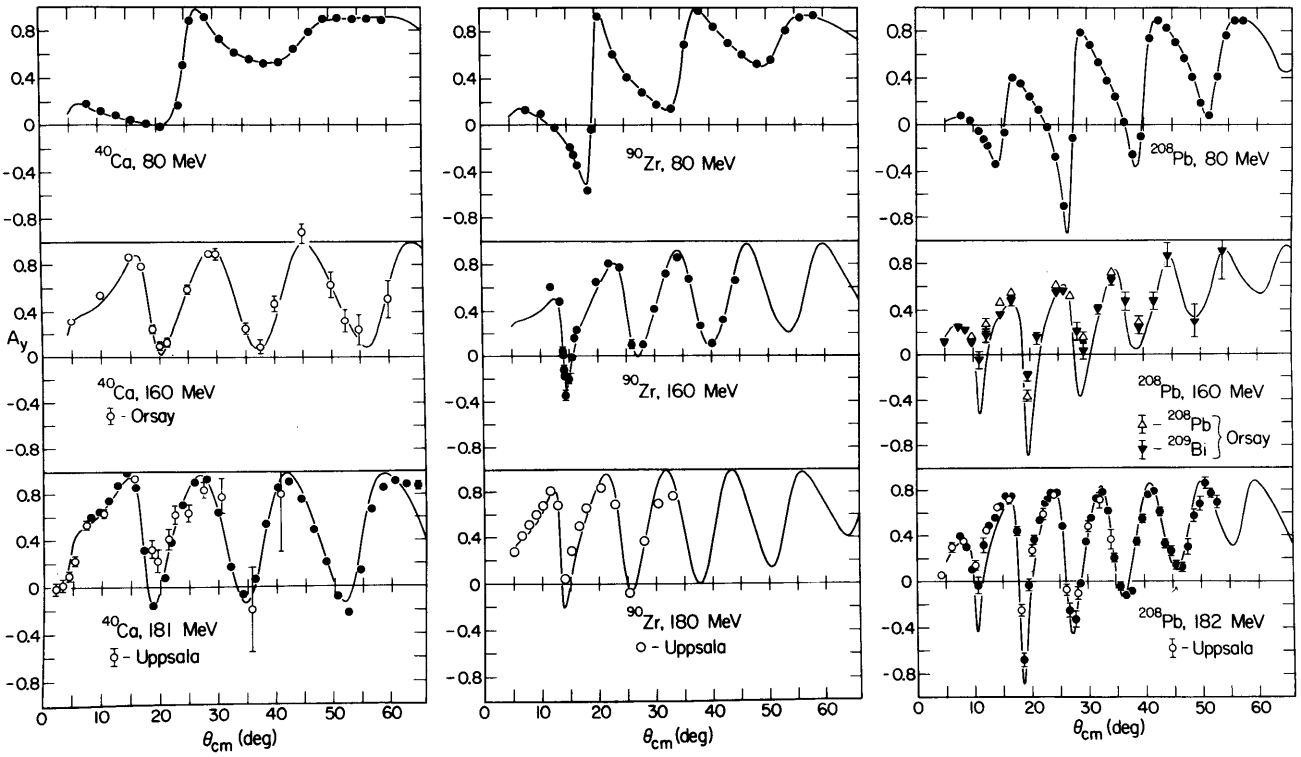

Figure 1. Analyzing powers A_y for 80, 160, and ~180 MeV protons elastically scattered from ^{40}Ca (left panel), ^{90}Zr (middle panel), and ^{208}Pb (right panel). Solid circles are IUCF measurements, open symbols (and all triangles) are from other sources as indicated. The curves are results of simultaneous optical-model fits to the A_y and associated σ data.

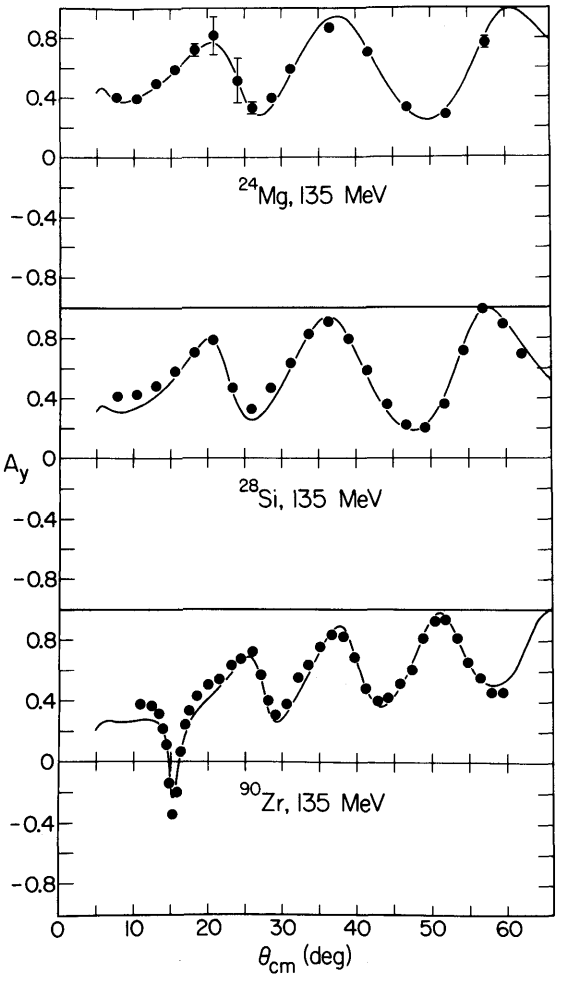

Figure 2. Analyzing powers for 135 MeV protons elastically scattered from ^{24}Mg, ^{28}Si, and ^{90}Zr (all IUCF data). The curves are results of simultaneous optical-model fits to the A_y and associated σ data.

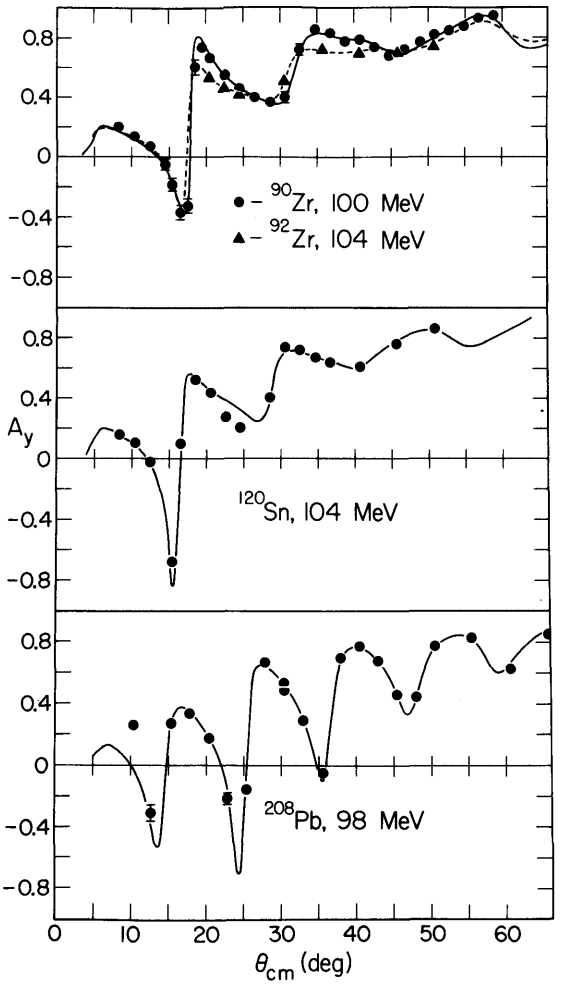

Figure 3. Analyzing powers for protons elastically scattered from ^{90,92}Zr, ^{120}Sn, and ^{208}Pb near 100 MeV bombarding energy (all IUCF data). The curves are results of simultaneous optical-model fits to the A_y and associated σ data.

and with investigating the excitation of high-spin states.[8]

The optical-model analysis presented here is conventional in the sense that the radial dependence of the optical potentials is of the Woods-Saxon (or Woods-Saxon derivative) type. Recently, evidence has been accumulating[9] that such a simple parametrization may not be adequate beyond a bombarding energy of about 150 MeV. In the present work, this aspect of the optical model is discussed only briefly; a detailed investigation of the implications of non-standard potential shapes for intermediate-energy proton scattering will be the subject of a future analysis.

The local optical potential used in the analysis of the data was parametrized as

$$U(r) = U_{coul}(r) - Vf_o(r) - iWf_w(r)$$

$$+ \frac{2.00}{r} [V_{so} \frac{d}{dr} f_{vso}(r) + iW_{so} \frac{d}{dr} f_{wso}(r)] \vec{L}\cdot\vec{\sigma}, \quad (1)$$

with Woods-Saxon form factors $f_x(r;r_x,a_x)$. Using the code[10] SNOOPY8, the potential parameters were adjusted for each case to fit simultaneously the angular distribution of the cross section, $\sigma(\theta)$, and the

analyzing power, $A_y(\theta)$. Relativistic effects were treated in an approximate way as described in Ref. 1. The starting parameters were taken from the "fixed-spin-orbit" fits to the cross-section data by Nadasen et al.[1]

Initially, all 12 parameters of the four nuclear potential terms (central and spin-orbit, real and imaginary parts) were varied in unconstrained "best-fit" searches on the data. Angular distributions of $A_y(\theta)$ calculated from these best-fit parameters are compared with the data in Figs. 1-3. The corresponding fits to the differential cross sections do not differ noticeably from those in Ref. 1 and for that reason are not reproduced here. The quality of fits to the $A_y(\theta)$ data is satisfactory overall, and excellent for most of the IUCF measurements.

Most of the geometry parameters of the complex spin-orbit (S.O.) potential exhibited little or no dependence on T_p. Hence, in order to reduce the scatter of individual parameter values with T_p, we proceeded to constrain successively more of the S.O. potential geometry to energy-independent values until finally all four parameters r_{vso}, a_{vso}, r_{wso}, and a_{wso} were held fixed in the parameter searches without deterioration in the overall quality of fit. Over the energy range $80 \leq T_p \leq 180$ MeV and target mass range $40 \leq A \leq 208$, these S.O. geometry parameters are well represented by the analytic relations (with T_p in MeV, r and a in fm):

$$r_{vso} = 0.920 + 0.0305A^{1/3}$$

$$a_{vso} = \begin{cases} 0.768 - 0.0012T_p, & T_p \leq 140 \text{ MeV} \\ 0.60, & T_p > 140 \text{ MeV} \end{cases} \quad (2)$$

$$r_{wso} = 0.877 + 0.0360A^{1/3}$$

$$a_{wso} = 0.62.$$

While constraining the geometry of the spin-orbit potential, we adjusted the remaining parameters to fit the data. The resulting values are presented as a function of the energy in Fig. 4 (solid symbols). The trend of most parameters with energy is readily apparent: central potential geometry parameters vary linearly with T_p and show no systematic dependence on target mass number A (with the possible exception of r_o

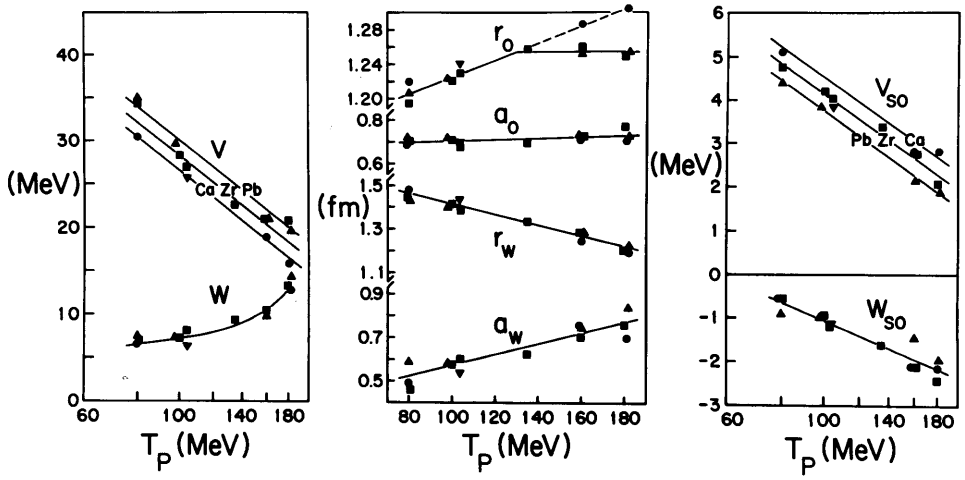

Figure 4. Energy dependence of the optical model parameters obtained in the present analyses of ^{40}Ca (circles), ^{90,92}Zr (squares), and ^{208}Pb (triangles) for the fixed spin-orbit geometry of eq. 2. The lines represent the average trend of the results described by eq. 3. Note the logarithmic proton energy scale for the central potential strengths (left panel) and the spin-orbit potential strengths (right panel).

at the higher energies); the strengths V and V_{so} of the real central and S.O. potentials decrease linearly with increasing $\log(T_p)$ and exhibit a noticeable dependence on A (consistent with an (N-Z)/A asymmetry); the imaginary central strength W increases rapidly with T_p at the higher energies; the magnitude of the imaginary S.O. strength W_{so} increases strongly with increasing $\log(T_p)$, becoming comparable to the real S.O. strength V_{so} near 200 MeV; neither W nor W_{so} shows any systematic A-dependence. The straight lines and curves in Fig. 4 represent least-squares fits to the potential parameters which resulted in the following functional dependences on T_p (in MeV) and A over the ranges $80 \leq T_p \leq 180$ MeV, $40 \leq A \leq 208$ (with V and W in MeV, r and a in fm):

$$
\begin{aligned}
V &= 105.5[1 - 0.1625\ell n(T_p)] + 16.5\,\frac{N-Z}{A} \\
r_o &= \begin{cases} 1.125 + 1.0\times10^{-3}T_p, & T_p \leq 130 \text{ MeV } (T_p \leq 180 \text{ MeV for Ca}) \\ 1.255, & T_p > 130 \text{ MeV (except for Ca)} \end{cases} \\
a_o &= 0.675 + 3.1\times10^{-4}T_p \qquad (3) \\
W &= 6.6 + 2.73\times10^{-2}(T_p - 80) + 3.87\times10^{-6}(T_p - 80)^3 \\
r_w &= 1.65 - 2.4\times10^{-3}T_p \\
a_w &= 0.32 + 2.5\times10^{-3}T_p \\
V_{so} &= 19.0[1 - 0.166\ell n(T_p)] - 3.75\,\frac{N-Z}{A} \\
W_{so} &= 7.5[1 - 0.248\ell n(T_p)]
\end{aligned}
$$

The specific functional relations chosen to represent the T_p and A dependences of the potential are phenomenological, i.e., not guided by any physical model. These T_p and A dependences determined in the present analysis of an extensive set of $\sigma(\theta)$ and $A_y(\theta)$ data differ quantitatively from those found in the earlier analysis of (predominantly) $\sigma(\theta)$ data by Nadasen et al.[1] (which included only a few $A_y(\theta)$ measurements). However, the qualitative behavior of the parameters with energy is fairly similar in the two analyses. The results of the present analysis thus largely substantiate the Nadasen results for the medium-energy proton optical potential within the specific framework of the conventional Woods-Saxon parametrization. In particular, we confirm the preliminary conclusions of Nadasen et al.[1] concerning the energy systematics of the proton S.O. potential and the need for a sizable imaginary S.O. component. Worthy of note are the relative energy and isospin dependences of the real S.O. and real central potentials: one finds $(1/V_{so})\delta V_{so}/\delta T_p = (1/V)\delta V/\delta T_p$ (in disagreement with a naive expectation[11] based on the different non-locality ranges for the two potential terms), and one finds an (N-Z)-dependence of V_{so} of opposite sign to that of V (in agreement with schematic model expectations[12]).

Recent phenomenological analyses[13] of 120-200 MeV $\vec{p} + {}^{12}C$ data, extending over a considerably larger range of momentum transfer than most medium-energy data (including the present data), as well as a global analysis of $\vec{p} + {}^{40}Ca$ data over the energy range $30 < T_p < 1000$ MeV in a relativistic Dirac-Hartree model,[14] have demonstrated that real central potential shapes deviating radically from the monotonic Woods-Saxon (W-S) form are consistent with, if not necessary to explain, the measurements for proton energies beyond ~150 MeV. Indeed, microscopic-model calculations[15,16] suggest that at such energies the proton-nucleus real central potential should have a pronounced depression just inside the nuclear surface. The strong energy dependence of some of the W-S geometry parameters found in the present analysis is likely to be caused (at least partly) by the unphysical constraint imposed on the analysis by the use of W-S form factors. The present parametrization is obviously adequate for providing a very good description of

existing $\sigma(\theta)$ and $A_y(\theta)$ data up to 180 MeV, as illustrated by the quality of the present fits. However, the prospective user of the present results (who may wish to generate distorted proton waves for reaction calculations) should be aware that the potential derived here may be only phase-shift equivalent to more physical, non-W-S potentials which also describe the elastic data, but may yield significantly different proton wave functions inside the nuclear surface.

Volume integrals of the complex central potential (W-S form) and of the complex S.O. potential (Thomas form) determined in the present analysis are presented as functions of bombarding energy T_p in Fig. 5 (solid symbols) for the constrained S.O. geometry case. In terms of the radial integrals $I_k \equiv 4\pi\int U_k(r)r^2dr$ for each of the four nuclear potential terms (k = o,w,vso,wso), the quantities shown are defined as $J_R \equiv I_o/A$, $J_I \equiv I_w/A$, $K_R \equiv I_{vso}/A^{1/3}$, and $K_I \equiv I_{wso}/A^{1/3}$. The shaded bands in Fig. 5 represent the values calculated from the analytical expressions for the potential parameters. The dashed and dot-dashed curves in Fig. 5 are microscopic predictions of the local optical potential based on a Brueckner-Hartree-Fock nuclear matter approach[15] (dashed curves) and results of the phenomenological Dirac-Hartree model[14] based on relativistic mean field theory (dot-dashed curves). For the real central potential, the form factors of these microscopic potentials are quite different from the W-S form chosen for the phenomenological parametrization. This accounts for the discrepancy between empirical and theoretical values for J_R. On

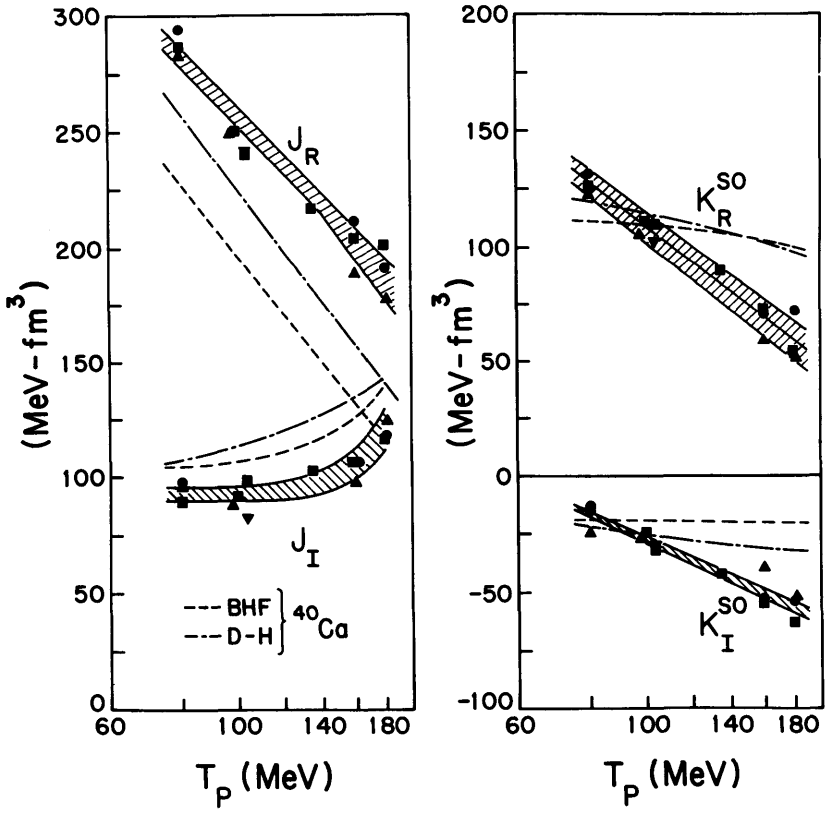

Figure 5. Energy dependence of the volume integrals of the complex central potential (left panel) and the complex spin-orbit potential (right panel). Symbols denote the individual results for the ^{40}Ca (circles), ^{90,92}Zr(squares), and ^{208}Pb (triangles). Shaded bands represent the variation of these quantities with T_p and A given by the average parametrization of the potentials (eqs. 2,3). Dashed curves are predictions of microscopically-based potential models.

the other hand, for the imaginary central and the complex S.O. potentials, the form factors of the phenomenological and microscopic models are sufficiently similar at all energies to make comparison of their volume integrals J_I, K_R, and K_I meaningful. However, the apparent similarity of empirical and theoretical J_I values masks some important intrinsic differences between the respective potentials: the microscopic imaginary potential tends to have a larger central strength but slightly shorter range. Also, the energy dependence found for the empirical S.O. potential volume integrals is stronger than is expected on the basis of the two microscopic models. Since the geometrical shapes of the S.O. potentials are fairly similar, this observation implies a considerable discrepancy in S.O. strength for energies beyond ~100 MeV: the empirical real S.O. strength falls off too fast with increasing T_p, while at the same time the empirical imaginary S.O. strength increases too rapidly in magnitude. These large differences are a direct consequence of the strong correlation between the surface-peaked S.O. potential and the assumed radial dependence of the central potential. Model calculations show that any appreciable deviation from the W-S form results in significant redistribution of real and imaginary S.O. strengths in the direction toward the microscopic model predictions. When viewed in this context, all volume integrals of the potentials determined in the present analysis are meaningful only in relation to the assumed W-S shape for the central potential.

1) A. Nadasen, P. Schwandt, P.P. Singh, W.W. Jacobs, A.D. Bacher, P.T. Debevec, M.D. Kaitchuck, and J.T. Meek, Phys. Rev. C 23, 1023 (1981).

2) P. Schwandt, H.O. Meyer, W.W. Jacobs, A.D. Bacher, S.E. Vigdor, M.D. Kaitchuck, and T.R. Donoghue, IUCF Preprint P-172 (submitted to Phys. Rev. C).

3) C. Rolland, B. Geoffrion, N. Marty, M. Morlet, B. Tatischeff, and A. Willis, Nucl. Phys. 80, 625 (1966).

4) A. Willis et al., J. Phys. 30, 13 (1969).

5) E. Hagberg, A. Ingemarsson, and B. Sundqvist, Physica Scripta 3, 245 (1971).

6) K. Kwiatkowski and N.S. Wall, Nucl Phys. A301, 349 (1978).

7) S. Kailas, P.P. Singh, A.D. Bacher, D. Friesel, C.C. Foster, P. Schwandt, and J. Wiggins, IUCF Preprint (1981) and contribution to this report.

8) S. Yen, R.J. Sobie, T.E. Drake, A.D. Bacher, G.T. Emery, W.P. Jones, D.W. Miller, C. Olmer, P. Schwandt, W.G. Love, and F. Petrovich, Phys. Lett. 105B, 421 (1981).

9) H.O. Meyer, P. Schwandt, G.L. Moake, and P.P. Singh, Phys. Rev. C 23, 616 (1981).

10) P. Schwandt, IUCF Report No. 81-3 (unpublished).

11) M.M. Giannini, J. Phys. G: Nucl Phys. 7, L29 (1981).

12) J.M. Moss, Phys. Rev. C 17, 813 (1978), and references therein.

13) P. Schwandt, H.O. Meyer, J.R. Hall, W.W. Jacobs, K. Kwiatkowski, P.P. Singh, and B.C. Clark, Bull. Am. Phys. Soc. 26, 635 (1981).

14) L.G. Arnold et al, Phys. Rev. C 25, 936 (1982); L.G. Arnold, B.C. Clark, R.L. Mercer, and P. Schwandt, Phys. Rev. C 23, 1949 (1981).

15) F.A. Brieva and J.R. Rook, Nucl. Phys. A291, 299 (1977); ibid., A291, 317 (1977); ibid., A297, 206 (1978); ibid., A307, 493 (1978).

16) H.V. von Geramb, F.A. Brieva and J.R. Rook, in Microscopic Optical Potentials, ed. von Geramb, Lecture Notes in Physics Vol. 89 (Springer, Berlin, 1979), p. 104.